

## Highlights

### **Reducing RES Droughts through the integration of wind and solar PV**

Boris Morin, Aina Maimó Far, Damian Flynn, Conor Sweeney

- RES droughts are analysed using 45 years of hourly wind and solar PV generation data
- RES droughts from C3S-Energy and ERA5-Atlite datasets are compared
- Adding solar PV to a wind-dominated system reduces RES drought frequency and duration
- Validated RES datasets are crucial to accurately identify RES drought extremes

# Reducing RES Droughts through the integration of wind and solar PV

Boris Morin<sup>a,\*</sup>, Aina Maimó Far<sup>a</sup>, Damian Flynn<sup>b</sup>, Conor Sweeney<sup>a</sup>

*<sup>a</sup>School of Mathematics and Statistics, University College Dublin, Belfield, Dublin  
4, Dublin, D04 V1W8, Ireland*

*<sup>b</sup>School of Electrical and Electronic Engineering, University College Dublin, Belfield,  
Dublin 4, Dublin, D04 V1W8, Ireland*

---

\*Corresponding author

*Email addresses:* `boris.morin@ucdconnect.ie` (Boris Morin ),  
`aina.maimofar@ucd.ie` (Aina Maimó Far), `damian.flynn@ucd.ie` (Damian Flynn),  
`conor.sweeney@ucd.ie` (Conor Sweeney)

---

## Abstract

Increasing the share of electricity produced from renewable energy sources (RES), combined with RES dependence on weather, poses a critical challenge for energy systems. This study investigates the importance of the balance between wind and solar photovoltaic (PV) capacity on periods of low renewable generation, known as RES droughts. Three different RES datasets are used to estimate the capacity factors for different scenarios of installed capacities for wind and solar PV power. The skill of the RES datasets is quantified by comparing capacity factor time series to observed hourly data and by assessing their representation of observed RES droughts. The RES datasets are used to generate a 45-year hourly time series of RES capacity factor, enabling analysis of the frequency, duration and return periods of RES droughts at a climatological scale. Results show the importance of using an accurate, validated RES dataset for RES drought risk assessment. The addition of solar PV capacity to a wind-dominated system results in a significant reduction in the frequency and duration of RES droughts, while also reducing extremes and seasonal RES drought patterns. These findings underscore the importance of diversification in RES capacity to enhance energy security and resilience.

*Keywords:* RES Drought, Wind Power, Solar PV Power, Renewable Energy Sources, Return Periods

---

## 1. Introduction

The EU aims to generate at least 69% of its electricity from renewable energy sources (RES) by 2030, up from 41% in 2022 [1]. While this transition is essential for reducing greenhouse gas emissions, it also highlights the challenge of managing the variability of weather-dependent energy sources such as wind and solar photovoltaic (PV) power. This challenge is amplified by the increasing electrification of energy sectors, which places greater demand on the power system and makes it more sensitive to meteorological conditions, both in historical [?] and future climates [?] [2]. Periods of low renewable generation, known as *Dunkelflaute* or RES droughts, pose significant risks to system adequacy and energy security, emphasising the need for a resilient energy system to meet both growing electricity demand and decarbonisation targets.

RES drought events do not have a fixed definition, with various approaches present in the literature. One common method defines a RES drought as a period during which the average capacity factor (CF) remains below a fixed threshold for a specified duration. For example, Kaspar et al. [3] used this method to investigate the shortfall risks of low wind and solar PV generation in Europe, with a focus on Germany, testing multiple CF thresholds and durations. Similarly, Mockert et al. [4] examined the link between weather regimes and RES droughts in Germany using a 48-hour rolling window under a threshold to define RES droughts. Similar fixed-threshold approaches have also been applied using CF series reconstructed through machine learning in regions such as Japan [5] and Hungary [6].

Alternative methods adjust the CF threshold dynamically over the year to account for seasonal variations in renewable production. Raynaud et al. [7] defined RES droughts as sequences of days with renewable electricity generation below a threshold that varies seasonally, a methodology later adapted for India [8]. Building on this, Kapica et al. [9] compared the likelihood of increased RES droughts in Europe under different climate models. Other studies have defined RES droughts based on deviations from daily mean production: Rinaldi et al. [10] applied these in the U.S. Western Interconnection to quantify the benefits of long-term storage, while Brown et al. [11] examined weekly timescales to explore meteorological influences on the most severe RES drought events. Another method defines RES drought indices based on metrics commonly used in hydro-meteorology to characterise RES droughts [12]. This approach identifies periods of unusually low generation relative to historical production levels, using the lowest production percentiles. Bracken et al. [13] used this approach to analyse RES droughts at different time scales in the U.S. [13], and Lei et al. [14] used it to quantify RES droughts in wind-PV-hydro systems in China.

In addition to examining periods of low renewable electricity generation, several studies also explore the periods when the imbalance between renewable generation and electricity demand (residual demand) is high. Raynaud et al. [7] showed the difference between RES droughts and high residual demand events in a hypothetical fully renewable system composed of wind, solar PV and run-of-the-river hydropower. Similarly, Allen and Otero [12] also defined a standardised index based on meteorological droughts to address residual demand, whose correlation to the electricity generation index is mostly negative (as expected, although quite low anticorrelations and even small positive correlations appear for some European countries). This index

was also applied to the U.S. by Bracken et al. [13], revealing a consistent increase in the RES drought magnitude when demand is considered, despite showing differing results across regions.

In this paper, the focus is exclusively on renewable electricity generation, to keep the focus on RES droughts driven by the weather. A fixed threshold approach is used to define RES droughts, which facilitates consistent inter-comparison between scenarios with different installed wind and solar PV capacities. The case study used in this paper is Ireland, a region where most RES generation comes from wind power and with ambitious targets for solar PV power expansion. This provides valuable insights into the potential benefits of adding solar PV installations in wind-dominated countries.

RES droughts are identified using onshore wind and solar PV CF time series. In this study, three different datasets are used and compared, all of which are driven by the ERA5 reanalysis [15]. Two of the datasets are part of C3S Energy (C3SE), an energy-based operational dataset produced by the EU Copernicus Climate Change Service [16]. One of the C3SE datasets provides CF time series aggregated at the national scale, while the other provides the CF time series at each grid point, at the ERA5 resolution of  $0.25^\circ$ . The third dataset produced by the authors was generated using the Atlite model [17], which converts the ERA5 atmospheric data to a generation time series using specified wind turbine and PV panel models. Atlite is an open-source tool developed by PyPSA [17] and has been used for estimating wind and solar PV generation in order to study RES droughts in Germany [4].

Generic datasets for wind and solar PV CF are often used for the quantification of RES droughts. Despite undergoing a general validation process, they are often not fully representative of each geographical location, and can show differences in the number of RES drought events subsequently identified [18]. This study evaluates the skill of a dataset developed for the European region (C3SE) when applied to a specific country; Ireland, [representative of Northwestern Europe](#). In particular, the analysis explores the impact of using a generic versus a tailored dataset on RES drought assessments, in the context of a transition from a wind-dominated system to one with a greater share of solar PV capacity.

The aim of this study is to answer two questions which are relevant for systems with a large share of RES generation:

- Do generic datasets have sufficient skill to reliably quantify RES drought events for specific countries?

- How does the integration of solar PV capacity into a predominantly wind-based system alter the characteristics of RES drought events?

The datasets used in this study are detailed in section 2, which describes their characteristics and relevance for evaluating RES droughts. Section 3 outlines the RES datasets used to simulate wind and solar PV generation and provides the methodology for defining and identifying RES drought events, including the thresholds and metrics applied. In section 4, the datasets are first verified against observed energy data to assess their accuracy, followed by an analysis of RES drought occurrences for two scenarios with different ratios of installed wind to solar PV capacities. Finally, section 5 offers a discussion of the results in the context of energy reliability and future planning, followed by the main conclusions and recommendations for further research.

## 2. Data

This study uses publicly available datasets to construct and validate the datasets for estimating the CF of wind and solar PV power. The primary data sources include: EirGrid and SONI, the transmission system operators (TSO) for the Republic of Ireland and Northern Ireland, respectively; the ERA5 reanalysis dataset; and the C3SE dataset.

### 2.1. Wind and solar PV Capacity and Availability

EirGrid, the TSO for the Republic of Ireland, and SONI, the Northern Ireland TSO, provide detailed datasets on all wind and solar PV farms across the island of Ireland (Republic of Ireland and Northern Ireland) from 1990 to the present [19]. These datasets include information such as each farm’s installed capacity, name, and connection date. To enhance the accuracy of this data, the longitude and latitude for each farm were manually determined through online searches. For simplicity, this data will be referred to as originating from EirGrid, as all-island data was directly obtained from EirGrid, and the combined regions of the Republic of Ireland and Northern Ireland will be referred to as Ireland throughout the remainder of this document.

The spreadsheet available from the EirGrid website contains two key variables: generation and availability. Generation and availability values are available from 2014 onward for wind power and from 2018 onward for solar PV power, although solar PV availability data only became present in the Republic of Ireland in 2023. Generation is the energy that a RES farm actually contributed to the grid, which may include limitations introduced by the

124 TSO to maintain grid stability, such as constraints and curtailment. Avail-  
 125 ability represents the energy that would have been generated from a RES  
 126 farm if no grid constraints had been applied, making it representative of the  
 127 weather-related response. This study focuses on availability for all analyses.

## 128 2.2. Atmospheric Variables

129 All of the datasets used in this study are driven by data from the ERA5 re-  
 130 analysis [15], produced by the European Centre for Medium-Range Weather  
 131 Forecasts (ECMWF). This global gridded dataset provides hourly atmo-  
 132 spheric variables from 1940 to the present at a horizontal resolution of  $0.25^\circ$ .  
 133 Table 1 lists the relevant ERA5 variables.

Table 1: ERA5 variables used to calculate wind and solar PV generation

ERA5 name	variable
100 metre zonal and meridional wind speed	$u_{100}, v_{100}$
2 metre temperature	$t2m$
Surface net solar radiation	$ssr$
Surface solar radiation downwards	$ssrd$
Top of atmosphere incident radiation	$tisr$
Total sky direct solar radiation at surface	$fdir$

## 134 2.3. C3S Energy

135 The EU Copernicus Climate Change Service developed the C3S-Energy  
 136 (C3SE) renewable energy dataset for Europe [16], using ERA5 atmospheric  
 137 variables and weather-to-energy models. This dataset provides hourly CF for  
 138 wind and solar PV power from 1979 to the present. The data are available  
 139 on the same grid as the ERA5 data, which has a horizontal resolution of  
 140  $0.25^\circ$ . The time series are also available for download at two aggregated  
 141 scales: regional (NUTS 2) and national.

142 The wind CF in C3SE was calculated using wind speeds at 100 ~~metres~~m  
 143 ( $u_{100}, v_{100}$ ) and a standard wind turbine model, the Vestas V136/3450, with  
 144 a fixed hub height of 100 ~~meters~~m. As data on wind turbine fleet locations  
 145 and specifications are difficult to obtain across Europe, C3SE assumes a  
 146 homogeneous distribution of wind turbines across the ERA5 grid. While  
 147 this approach does not capture the precise capacity factors reported by grid  
 148 operators, it provides a well-correlated time series that effectively represents

the impact of ~~climate~~weather variability on wind power generation. The C3SE solar PV CF was also calculated for the ERA5 grid. It is derived from meteorological data, including surface solar radiation downwards (*ssrd*) and air temperature (*t2m*), using a reference solar PV plant model. This model incorporates empirical calculations for key system components, such as optical losses, ~~module efficiency, and inverter~~the electrical characteristics of the power module and the power curve of the PV inverter. The final CF accounts for a mix of module orientations typical for each location [20].

### 3. Methods

This study analyses RES droughts using onshore wind and solar PV CF time series from three datasets: two from C3SE; one based on national-level data (C3S NAT) and the other on grid-level data (C3S GRD), and a third dataset derived using the Atlite model (ATL).

#### 3.1. C3S Energy National: C3S NAT

The C3S NAT dataset is created by combining two inputs provided by C3SE at the corresponding NUTS levels: Republic of Ireland (NUTS0: IE) and Northern Ireland (NUTS2: UKN0). The two inputs are combined, using the actual installed capacity as weights. This dataset assumes that RES generation occurs at every ERA5 grid point in Ireland.

#### 3.2. C3S Energy Gridded: C3S GRD

The C3S GRD dataset uses, as inputs, the actual locations of the RES farms in Ireland, and the CF from C3SE over the ERA5 grid. For each farm, the CF from the nearest grid point on the C3SE dataset was selected. A weighted average of the CF associated with each farm, using the farm's installed capacities, was used to produce the ~~total~~combined CF time series.

#### 3.3. Atlite: ATL

The ATL dataset is produced using the Atlite model. Atlite allows the user to define the wind turbine power curve and PV panel model to use when converting weather variables to wind and solar PV generation. The Atlite model takes as inputs the locations of RES farms and ERA5 weather variables: wind speed at 100 ~~metres~~m ( $u_{100}$ ,  $v_{100}$ ) for wind generation, and radiation variables (*ssr*, *ssrd*, *tisr*, and *fdir*) along with air temperature (*t2m*) for solar PV generation. The output of the Atlite model is a generation



time series, which is divided by the total capacity to transform it back into [a](#) CF. The selection of the wind turbine power curve and PV panel model represents the key difference between this dataset and C3S GRD. This study identifies the most appropriate wind turbine power curve to use from the 121 power curves, each at five different levels of smoothing, made available by Renewables.ninja [21], and selects the PV panel model out of the options available within Atlite.

### 3.4. Energy Scenarios

The three datasets provide ~~CF~~ time series for both wind and solar PV [CF](#). In addition to analysing the CF of wind and solar PV separately, a combined CF was computed for each dataset by averaging wind and solar PV CF, weighted by their installed capacities at the end of 2023 (5.9 GW for wind power and 0.6 GW for solar PV power). This configuration is referred to as the 91W-9PV scenario, reflecting the distribution of 91% wind and 9% solar PV capacity. Given that solar PV capacity in Ireland is low in 2023, and to explore how a more balanced distribution of wind and solar PV capacities might impact RES droughts, this study also considered a second scenario, referred to as 57W-43PV, where the installed solar PV capacity is assumed to increase to 8.6 GW, while wind capacity rises to 11.45 GW. These values are based on targets outlined in the roadmap published by the 2024 Climate Action Plan [22]. This study does not include offshore wind in the analysis. Recent reports suggest that even by 2030, Ireland is unlikely to have any significant new offshore wind farms, with projected offshore capacity expected to remain near zero using realistic scenarios [23].

New time series were generated for both the ATL and C3S GRD solar PV datasets, incorporating a revised distribution of installed capacity across Ireland as specified in the roadmap [24]. For wind power, the CF time series remains unchanged, as significant shifts in the location of wind farms are not expected. In total, twelve CF time series were analysed in this study, six for individual wind and solar PV CF (three datasets for each source) in the 91W-9PV scenario, and an additional six time series that include the combined CF for 91W-9PV and 57W-43PV scenarios across the different datasets.

It is important to note that the specific capacity values used in this study are illustrative and are not intended to reflect accurate future realities. Instead, they serve to explore the impact of transitioning from a wind-dominated system (91W-9PV) to a more evenly distributed system (57W-43PV). This approach allows for a comparative analysis between the two

219 scenarios, assessing how the balance of RES capacity affects the occurrence  
220 of RES droughts.

221 In summary, for each of the three datasets (ATL, C3S GRD and C3S  
222 NAT) four energy scenarios are examined:

- 223 • Wind Power - based on ~~the~~ actual capacity at the end of 2023
- 224 • Solar PV Power - based on ~~the~~ actual capacity at the end of 2023
- 225 • Combined RES / 91W-9PV - based on ~~the~~ actual capacity at the end  
226 of 2023
- 227 • Combined RES / 57W-43PV - based on ~~the~~ projected capacity for 2030

### 228 3.5. RES Drought Definition

229 In this study, a RES drought event was defined as occurring when the  
230 24-hour moving average of CF remains below a fixed threshold of 0.1 for a  
231 period of longer than 24 hours. By using a 24-hour moving average, fewer  
232 but longer-lasting events were captured compared to using the raw CF time  
233 series, which can be more sensitive to short-term fluctuations. The 24-hour  
234 rolling average also avoids potential masking of day-long events due to their  
235 start time. A fixed threshold approach was chosen in this study to enable  
236 consistent inter-comparison between datasets.

237 The moving average approach smooths out short-term fluctuations, so  
238 that brief periods above the threshold do not interrupt an otherwise continu-  
239 ous low-CF period (Fig. 1). This means that a single hour above the threshold  
240 does not "break" a RES drought event if it is surrounded by prolonged low-  
241 generation hours. As a result, fewer but longer-lasting RES drought events  
242 are identified, which may better reflect actual conditions where energy supply  
243 constraints persist over extended periods.

## 244 4. Results

### 245 4.1. Verification

246 The accuracy of the datasets used in this study was verified against  
247 national generation data, before continuing to the analysis of RES droughts.  
248 For the verification process, ~~time-varying~~ time varying values of installed  
249 capacity were used to account for changes in RES development over the  
250 verification period. This ~~step allowed us to assess how well the datasets~~

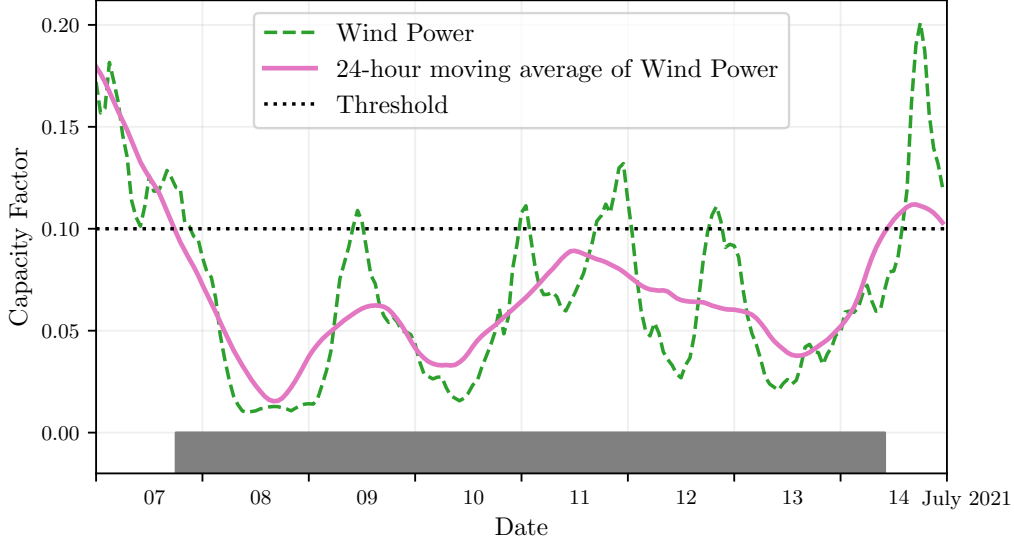


Figure 1: Wind time series of CF (green) and its 24-hour moving average (pink) from the 7th to the 15th of July 2021. The black dashed line indicates the CF threshold. The grey bar shows the period identified as a wind drought under our definition

251 ~~represent the production of renewable energy by comparing them against~~  
 252 ~~observed data. This validation step evaluates how well the datasets repre-~~  
 253 ~~sent actual renewable~~ energy production generation profiles ~~by comparing~~  
 254 ~~them against observed data. The overall statistical distribution of CF values~~  
 255 ~~for wind (2014–2023) and solar PV (2023) is presented in the violin plots~~  
 256 ~~in Fig. 2. These plots illustrate the density of CF values for each dataset,~~  
 257 ~~highlighting their differences and alignment with observations. The results~~  
 258 ~~indicate that ATL aligns more closely with~~ OBS observations ~~for wind, while~~  
 259 ~~all datasets exhibit similar distributions for solar PV.~~

#### 260 4.1.1. Wind Energy

261 The C3S datasets use the Vestas V136/3450 wind turbine power curve  
 262 (Fig. 3a). The Atlite model allows the user to specify the power curve.  
 263 We considered the 121 power curves available for download from Renew-  
 264 ables.ninja [21]. For each power curve, Renewables.ninja also provides four  
 265 associated smoothed power curves. The smoothing is done using a Gaussian  
 266 filter with different standard deviations that depend on the wind speed. A  
 267 separate wind CF time series for Ireland was generated for each of the wind

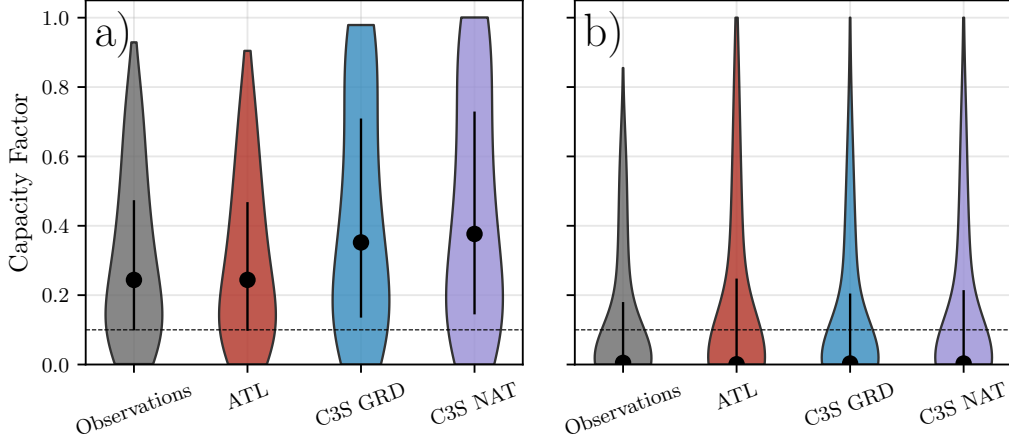


Figure 2: Violin plots of CF distributions for a) wind and b) solar PV for the Observations (grey) and the three datasets: ATL (red), C3S GRD (blue), and C3S NAT (purple). The black dot shows the median values, while the black vertical lines represent the first and third quartiles. The black dashed line indicates the threshold of 0.1 used in the study to identify RES droughts

268 turbine power curves and smoothing levels.

269 The performance of each CF time series is then assessed based on four skill  
 270 scores: correlation coefficient (CC), root mean square error (RMSE), mean  
 271 bias error (MBE), and the percentage of overlap. The percentage of overlap  
 272 quantifies the similarity between the observed and modelled distributions. It  
 273 is a positively oriented skill score, where 100% shows full agreement between  
 274 the two distributions, and 0% indicates no overlap. The histograms of hourly  
 275 CF values for the most recent decade (2014-2023) are used to calculate this  
 276 skill score.

277 Based on these metrics, the most representative power curve for Ireland  
 278 is the Enercon E112.4500 power curve with the  $0.3w$  smoothing filter. The  
 279 smoothing of the wind turbine power curve represents losses associated with  
 280 each turbine, as well as losses such as wake effects between turbines, which  
 281 are important when modelling wind energy on larger spatial scales. The  
 282 histogram in Fig. 3b shows that the C3SE power curve tends to underestimate  
 283 low CF values and overestimate higher ones, whereas the smoothed ATL  
 284 power curve more closely follows the observed wind availability data. This  
 285 is further supported by the percentage of overlap which is higher for ATL  
 286 (97.2%) than for C3SE (83.2%), indicating better agreement with observed

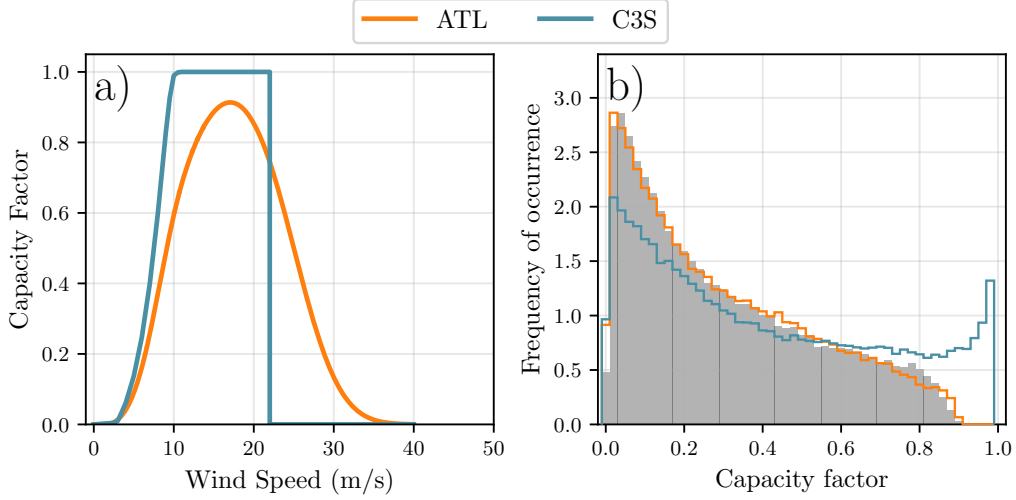


Figure 3: a) Power curves of the Enercon E112.4500 with a 0.3w smoothing filter used by the ATL dataset (orange) and the Vestas V136/3450 used by the two C3S datasets (blue) b) Histograms of wind CF for Ireland for the ATL dataset (orange), the C3S datasets (blue) and Observed (shaded)

287 data.

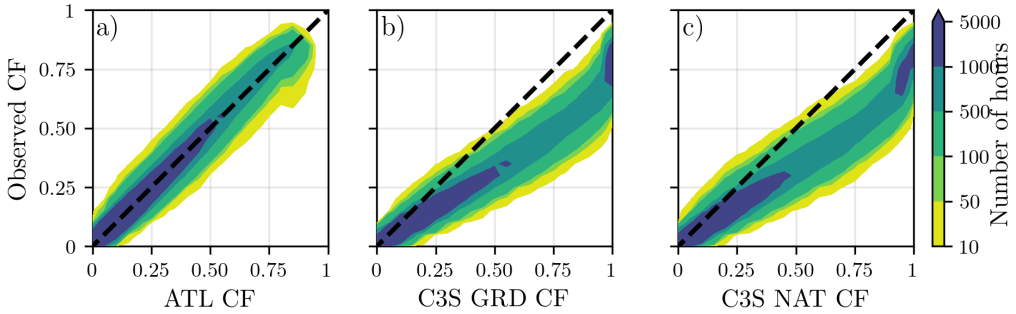


Figure 4: Wind CF density plot of the observed CF (vertical axes) and modelled (horizontal axes) CF data for the a) ATL, b) C3S GRD and c) C3S NAT datasets

288 The effect of the difference between the power curves is also visible in  
 289 Fig. 4, which shows a density plot of wind CF values. The two C3S datasets  
 290 are shown to overestimate the observed CF, whereas the ATL dataset is in  
 291 good agreement with the observed data. The skill scores presented in Table 2

show that ATL performs better than the two C3S datasets for all of the skill scores.

	ATL	C3S GRD	C3S NAT
<b>CC</b>	0.981	0.972	0.970
<b>RMSE</b>	0.045	0.177	0.162
<b>MBE</b>	-0.003	0.137	0.121

Table 2: Skill scores for wind power for the three datasets compared to observed data

Fig. 5 shows the average annual number of wind drought events during the 2014 to 2023 validation period. The figure reveals that ATL presents the best overall agreement with the observed frequency and duration of wind drought events. This pattern is particularly evident for shorter-duration events, which are the most frequent.

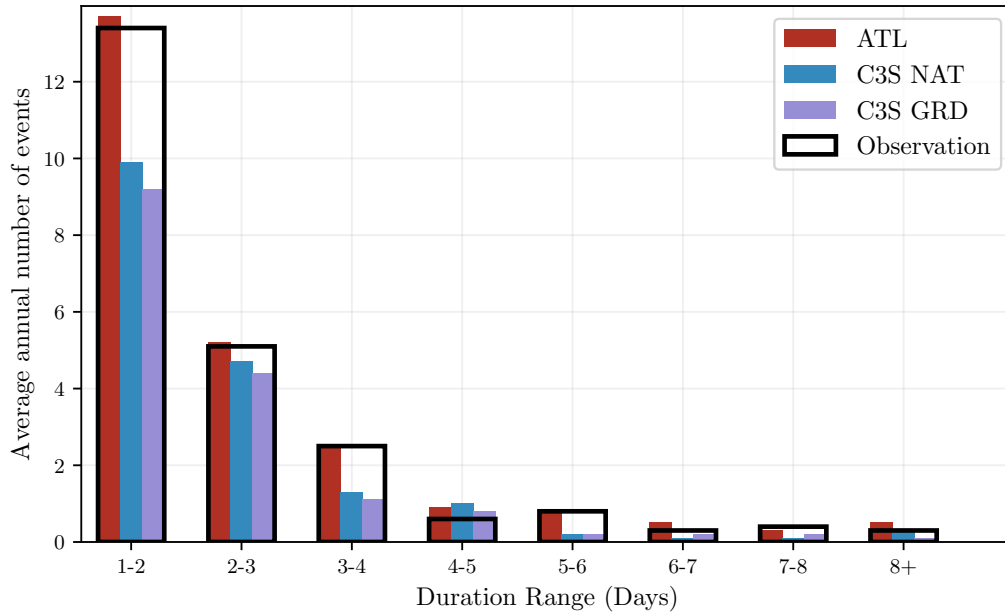


Figure 5: Average annual number of wind drought events for ATL (red), C3S GRD (blue), C3S NAT (purple), and the observed data (black outline). The wind droughts are identified from 2014 to 2023, considering the actual capacity of the system at any given time

~~This verification for~~ Verification of wind generation data highlights the importance of selecting a representative wind turbine power curve for the

301 region being analysed. The ATL dataset, which uses a representative wind  
 302 turbine power curve, is skilled at reproducing wind CF and RES droughts  
 303 ~~over~~ across Ireland. On the other hand, the power curve used for both  
 304 C3S GRD and C3S NAT is not representative for Ireland, as it severely  
 305 overestimates generation, underestimating the occurrence of RES droughts.  
 306 This highlights a problem with using generalised datasets for analysing RES  
 307 droughts: biases severely affect their ability to accurately reproduce RES  
 308 drought events. The skill scores for the three datasets (~~Tab.~~ Table 2) show  
 309 only a small difference in their ability to reproduce the changes in CF, as seen  
 310 by their similar CC scores. However, their ability to reproduce the actual  
 311 CF values is much lower than that ~~of~~ for ATL, with RMSE scores almost  
 312 four times ~~bigger~~ higher than for the two C3S datasets. There is a clear bias  
 313 towards an overestimation of CF, seen in the MBE values, which leads to  
 314 ~~the an~~ underestimation of RES droughts. ~~This highlights the need,~~ which  
 315 highlights the strong motivation to use regionally verified ~~datasets~~ models to  
 316 assess RES droughts.

#### 317 4.1.2. Solar PV Energy

318 The Atlite model allows the user to select certain PV panel characteristics.  
 319 In this study, the three PV panel types available in the Atlite model were  
 320 considered (CSi, CdTe, Kaneka). Following the same methodology as in the  
 321 previous section, the three available models were compared using four skill  
 322 scores (CC, RMSE, MBE, and the percentage of overlap). Based on the best-  
 323 performing metrics, the Beyer PV panel model was selected [25], using the  
 324 Kaneka Hybrid panel option. For all solar PV farm locations, the azimuth  
 325 angle is fixed at 180° (due south), and the optimal tilt angle option is applied.

326 The solar PV installed capacity available on the spreadsheets from Eir-  
 327 Grid represents the Maximum Export Capacity (MEC) and does not ac-  
 328 curately reflect the installed solar PV capacity. To enable actual solar PV  
 329 generation potential to be modelled correctly, installed capacities were set at  
 330 1.4 times the MEC values. This scaling factor was estimated by analysing  
 331 proprietary data from individual solar PV farms provided by EirGrid, which  
 332 showed that, on average, assuming that the installed capacities of farms ex-  
 333 ceed their MEC values by 40% yields the best agreement with the observed  
 334 availability.

335 Fig. 6 shows that the three datasets have a similar tendency to overesti-  
 336 mate the CF compared to the observed values, especially for high CF values.  
 337 The skill scores presented in Table 3 indicate that C3S GRD and C3S NAT

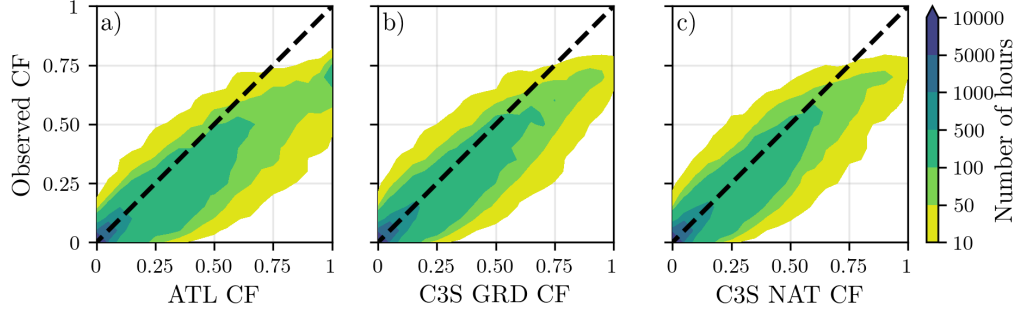


Figure 6: Solar PV CF density plot of the observed (vertical axes) and modelled (horizontal axes) CF series for the a) ATL, b) C3S GRD and c) C3S NAT datasets

perform better than ATL for solar PV CF, with lower RMSE and MBE, and higher CC scores. This may be due to the statistical approach taken by C3SE for the orientation of the PV panels.

	ATL	C3S GRD	C3S NAT
<b>CC</b>	0.921	0.931	0.931
<b>RMSE</b>	0.119	0.090	0.113
<b>MBE</b>	0.046	0.027	0.021

Table 3: Skill scores for solar PV CF for the three datasets compared to observed data

Fig. 7 shows the number of solar PV drought events during the 2023 validation period across different duration ranges. The figure reveals partial agreement between the three datasets and the observed data, with consistent results noticed for duration ranges of 1-2, 3-4, 7-8, and 8+ days. However, discrepancies appear in the other ranges, where the datasets diverge from the observed data. The main challenge in validating solar PV data stems from the recent installation of a large share of Ireland’s solar PV capacity, with over 65% of the total solar PV capacity installed in 2023. This results in uncertainties in solar PV generation data and the actual generating capacity in the first few months after each farm is connected. Overall, C3S GRD performs slightly better than the other datasets in reproducing observed solar PV drought events.



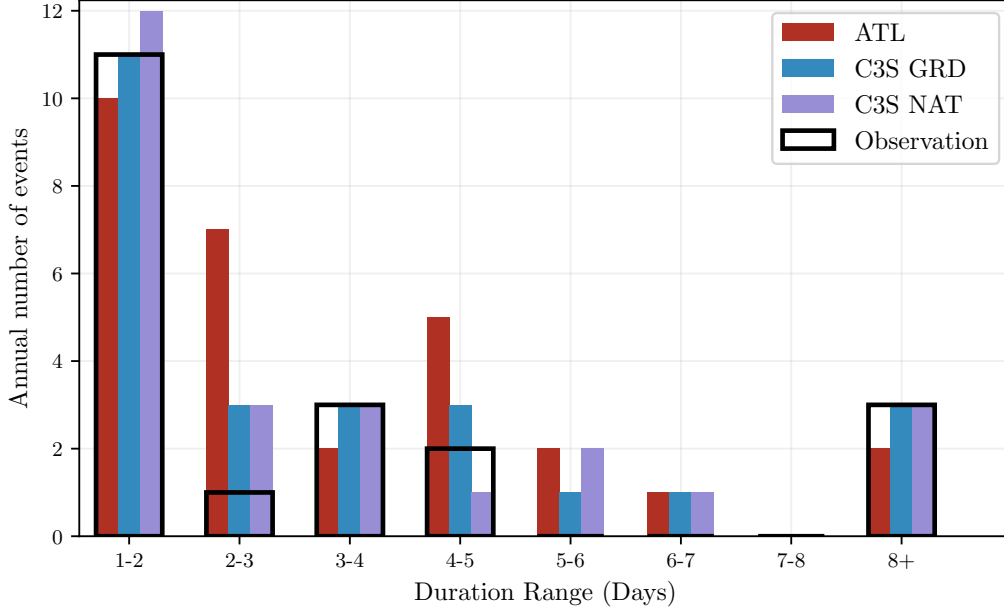


Figure 7: Number of solar PV drought events for ATL (red), C3S GRD (blue), and C3S NAT (purple) and the observed data (black outline). The solar PV droughts are identified for 2023, considering the actual capacity of the system at any given time

#### 4.2. Analysis

In this section, RES droughts are analysed by calculating the frequency and duration of ~~RES drought events, the return periods for different RES drought durations, and the seasonality of RES drought events.~~ Understanding the characteristics and timing of RES drought events enables system operators to optimally plan for reserve capacity requirements, ensuring grid stability and security of supply events, their return periods, and their seasonality. By examining both the frequency of occurrence and duration of these events, TSOs can better assess the need for alternative fossil fuel-based generation, long-duration energy storage, demand-side measures, and enhanced interconnections with neighbouring power systems to ensure adequate supply in a cost-effective manner. Results are presented for the three datasets, ~~allowing their differences on which clearly illustrate how different modelling assumptions influence the characterisation of RES droughts to be clearly identified.~~

RES drought events are evaluated under two different scenarios with fixed installed capacities: the 91W-9PV scenario, with 5.9 GW of wind capacity

369 and 0.6 GW of solar PV capacity; and the 57W-43PV scenario, where wind  
370 capacity comprises 11.45 GW and solar PV capacity increases to 8.6 GW.  
371 Both scenarios were driven by 45 years of ERA5 data. Using the RES drought  
372 identification process described in Section 3.5, wind and solar PV droughts  
373 are first analysed separately before presenting the results for combined (wind  
374 + solar PV) RES droughts under both scenarios.

#### 375 4.2.1. Annual Number of RES Droughts

376 The first part of the analysis examines the annual number of RES drought  
377 events. When only wind energy is considered (Fig. 8a), the number of RES  
378 drought events decreases as the duration range increases, with very few events  
379 lasting more than seven days. In contrast, for solar PV energy (Fig. 8b), RES  
380 drought frequency declines from one to eight days and then slightly increases  
381 for longer durations. This behaviour is attributable to Ireland’s high-latitude  
382 location, where reduced sunlight in winter (from November to March) leads  
383 to consistently low solar PV output.

384 Moreover, the comparison between wind and solar PV results indicates  
385 that the median, first, and third quartiles for solar PV are consistently higher  
386 than or equal to those for wind. This is expected, given that solar PV gener-  
387 ation is inherently lower, zero at night, and limited by the solar cycle. When  
388 wind and solar PV are combined under the 91W-9PV scenario (Fig. 8c), the  
389 results closely mirror those of wind alone, due to the dominance of wind power  
390 in the current energy mix. However, in the 57W-43PV scenario (Fig. 8d), a  
391 marked reduction in RES drought events is observed across all datasets, with  
392 a decrease of the total number of events of 56% for ATL, 52% for C3S GRD,  
393 and 50% for C3S NAT, demonstrating the beneficial effects of a more equal  
394 share of wind and solar PV capacity.

395 The consistently higher RES drought counts reported by the ATL dataset,  
396 compared to the C3S datasets, underscore the importance of wind turbine  
397 power curve representation when quantifying RES droughts. Whereas the  
398 three datasets agree on the overall effect of balancing the share of wind and  
399 solar PV generation, they differ at a quantitative level, which has crucial  
400 implications for energy planning.

#### 401 4.2.2. Return Periods of RES Drought Duration

402 RES drought events identified over the 45-year period were used to calcu-  
403 late the return periods for different RES drought durations. A return period  
404 is the estimated average time interval between events of a specified duration

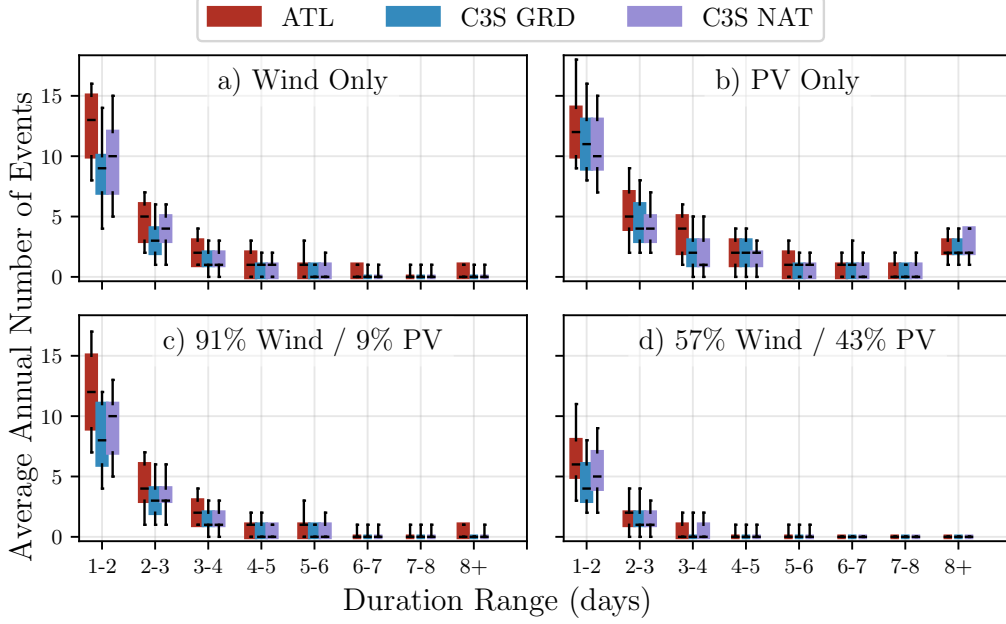


Figure 8: Average annual number of RES droughts (from 1979 to 2023) for a) Wind, b) solar PV, c) 91W-9PV and d) 57W-43PV for ATL (red), C3S GRD (blue), and C3S NAT (purple). The x-axis represents duration ranges in days (lower bound included), while the y-axis indicates the annual number of events. The boxes display the first and third quartiles and the median is marked by a black line. The whiskers indicate the 5th and 95th percentiles

(not to be confused with the frequency of their occurrence within a fixed time frame). Fig. 9 shows the return periods for different RES drought durations, which can be used to capture the most extreme events affecting the system. Understanding their return periods is crucial ~~as extreme yet to inform~~ decision makers about the trade-off between the risk of extreme events and the associated costs of mitigation measures. Extreme but rare RES droughts pose the toughest challenge to energy security by placing significant strain on the conventional backup sources necessary to maintain security of supply during these events.

The duration of wind droughts (Fig. 9a) increases in a log-linear fashion across the three datasets. The log-linear trend indicates a predictable relationship between wind drought duration and occurrence, with longer wind droughts becoming exponentially less likely as duration increases. In the

case of solar PV droughts (Fig. 9b), Atlite behaves differently than the two C3S datasets. The ATL dataset show a generally log-linear increase. For C3S GRD and C3S NAT, the duration of PV droughts increases in a log-linear pattern for events lasting less than 16 days. Beyond this duration, there is a sharp rise in solar PV drought duration for events up to a one-year return period. This sudden increase again reflects the impact of extended periods of low PV generation during winter in Ireland. The difference between the ATL and the C3S results arises from differences in the datasets near the threshold of 0.1 CF. ATL remains slightly above the threshold more frequently during these conditions, leading to shorter, more fragmented RES drought events. In contrast, C3S GRD and C3S NAT tend to fall below the threshold in similar conditions, resulting in longer continuous RES drought periods, especially during winter.

Under the 91W-9PV scenario (Fig. 9c), the combined RES drought return periods mirror those for wind alone, reflecting the dominance of wind in the current energy mix. In contrast, the 57W-43PV scenario (Fig. 9d) shows a dramatic reduction in RES drought durations, suggesting that a more balanced share of wind and solar PV capacity can substantially mitigate the frequency of prolonged RES drought events. For example, the return period for a five-day RES drought event (shown by the vertical dashed lines in Fig. 9) increases from roughly six months for the 91W-9PV scenario, to four years for the 57W-43PV scenario ~~in~~ for the ATL dataset, and from about fifteen months to around five years ~~in~~ for the two C3S datasets. This result indicates that the complementarity between wind and solar PV plays a crucial role in reducing the occurrence of RES drought events in a diversified energy portfolio.

Across Fig. 9a, c, and d, the return periods in the ATL dataset are consistently higher than those in the two C3S datasets. For instance, in the 91W-9PV scenario (Fig. 9c), an event with a one-year return period lasts six days in the ATL dataset, compared to only five days in the C3S datasets. This difference underscores the importance of dataset selection when quantifying RES droughts, as each dataset’s assumptions and parametrisations significantly influence RES ~~droughts~~ drought duration estimates. Additionally, in all four graphs, the similarity between results from the two C3S datasets suggests that assumptions in the ATL dataset, such as wind turbine power curve selection and PV panel specifications, have a greater impact on RES drought duration estimates than the precise geographic distribution of RES farms when studying the return periods of RES droughts.

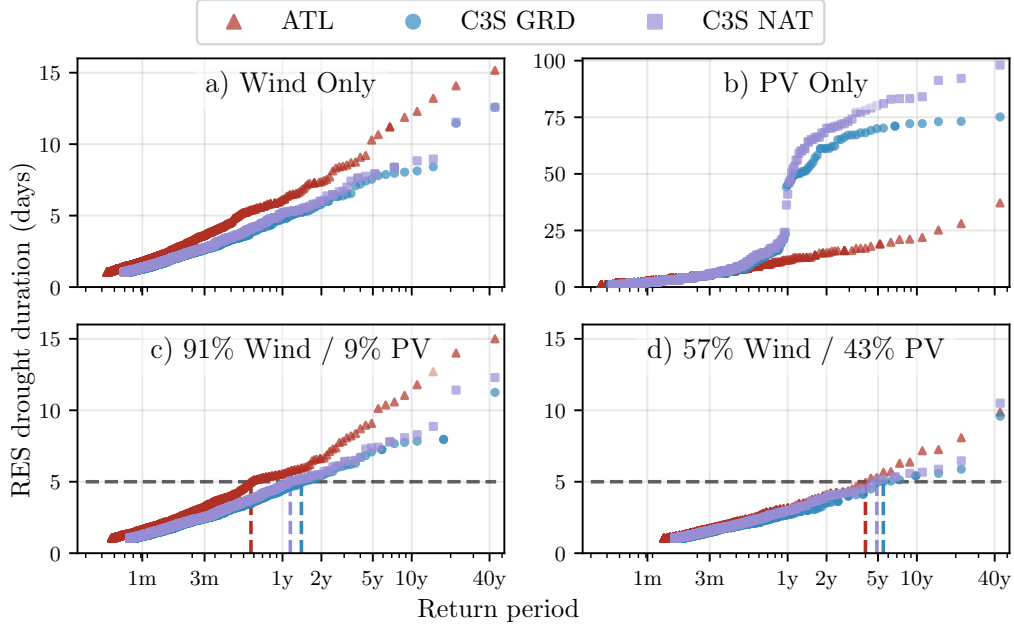


Figure 9: Return periods of the duration of RES droughts (from 1979 to 2023) for a) Wind, b) Solar PV, c) 91W-9PV and d) 57W-43PV for ATL (red triangle), C3S GRD (blue circle), and C3S NAT (purple square). The x-axis represents the return period time in a log-scale and the y-axis indicates the duration of RES drought associated with it. The horizontal dashed line marks the 5-day return period, with coloured vertical dashed marking its return period for each dataset

456 The return periods calculated from the three datasets show large differ-  
 457 ences, in particular for the more extreme events with longer return periods.  
 458 The C3S datasets produce shorter RES drought durations for these events,  
 459 which would have the largest impact on the power system. This shows that  
 460 system planning based on the wrong datasets could yield an underestimation  
 461 of the duration of extreme RES droughts, potentially leading to shortages  
 462 linked to undersized reserve capacity.

#### 463 4.2.3. Seasonal Distribution of RES Droughts

464 The seasonal analysis of RES droughts is based on the percentage of hours  
 465 in each month classified as part of a RES drought event. Wind droughts tend  
 466 to be more frequent during summer, whereas solar PV droughts are more  
 467 common in winter due to reduced sunlight. By comparing these seasonal pat-  
 468 terns across different datasets and energy scenarios, this study examines how

~~dataset-specific assumptions and variations in capacity mix affect the overall~~  
differences in model assumptions and capacity mix influence the characteri-  
sation of RES drought events. In Northwestern Europe, winter droughts are  
primarily driven by variations in wind generation, whereas summer droughts  
are mainly related to solar generation. This seasonal analysis is critical to  
ensure a cost-effective balance between generation and demand throughout  
the year.

For the wind-only scenario (Fig. 10a), the ATL dataset exhibits a pro-  
nounced seasonal pattern, with about 24% of summer hours (June, July,  
August) identified as RES droughts compared to only 4% in winter (Decem-  
ber, January, February). This strong seasonal signal is less evident in the C3S  
datasets, which suggests that the differences in the underlying wind power  
curves play a significant role. In ATL, CF near or below the 0.1 threshold  
occurs at relatively higher wind speeds, resulting in a higher count of RES  
drought hours during the summer months. In contrast, solar PV droughts  
(Fig. 10b) display an opposite seasonal trend. Across all datasets, over 60%  
of winter hours are classified as solar PV droughts, reflecting the naturally  
low solar irradiance in Ireland during winter.

ATL tends to record a slightly higher percentage of RES drought hours  
for wind and a marginally lower percentage for solar PV relative to the C3S  
datasets. These differences highlight how dataset-specific assumptions, such  
as the treatment of wind turbine power curves and PV panel characteristics,  
influences the seasonal dynamics of RES droughts.

The 91W-9PV scenario (Fig. 10c) shows patterns similar to the ones for  
wind droughts (Fig. 10a). However, in the 91W/9PV scenario, the number  
of hours classified as RES droughts in summer decreases slightly compared to  
the wind-only scenario. This reduction can be explained by the contribution  
of solar PV generation during the summer months in the 91W-9PV scenario,  
even though it constitutes only 9% of total capacity. Since the number of RES  
drought hours for solar PV in summer is near zero, this small contribution  
has a noticeable impact on reducing overall RES drought hours. In the 57W-  
43PV scenario (Fig. 10d), all three datasets show a reduction in monthly RES  
drought frequency. Annual reductions in median RES drought frequency are  
observed across the datasets, dropping from 14% to 5% for ATL, from 8% to  
3% for C3S GRD, and from 9% to 4% for C3S NAT. The balanced mix of wind  
and solar PV power in this scenario reduces the seasonal signal overall and  
significantly decreases the percentage of RES drought hours in the summer.

The seasonal variations of RES droughts observed in this study have im-

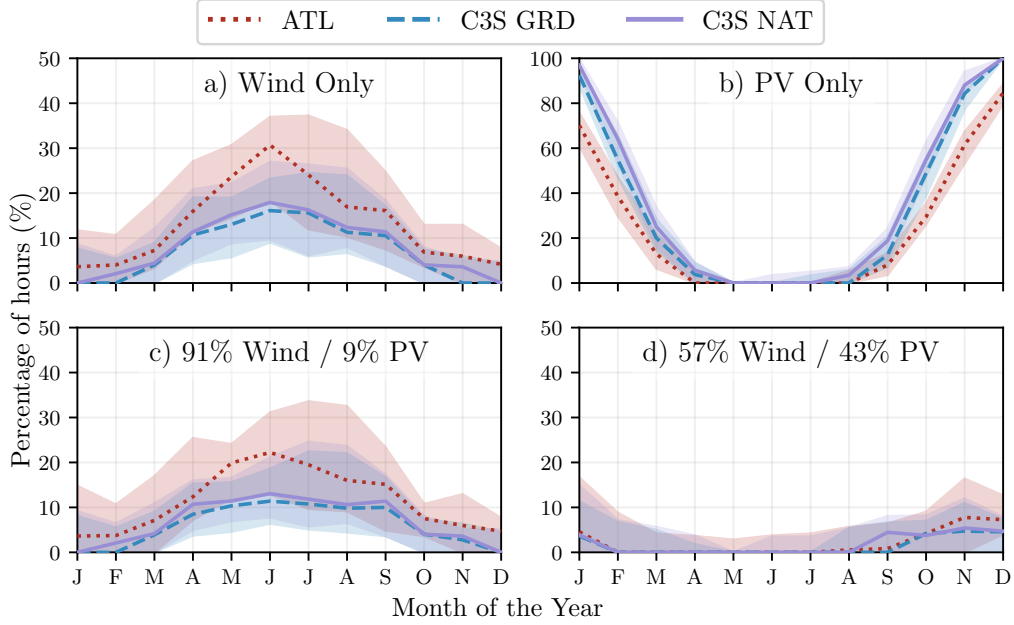


Figure 10: Percentage of hours in a month which are part of a RES drought (from 1979 to 2023) for a) Wind, b) Solar PV, c) 91W-9PV and d) 57W-43PV for ATL (red dotted), C3S GRD (blue dashed), and C3S NAT (purple solid). The x-axis represents the month of the year, and the y-axis indicates the percentage of hours. Lines correspond to the median values and the area between the first and third quartiles is shaded. Note the different y-axis scale for b).

507 portant implications for energy planning. Energy demand peaks in winter  
 508 for Northern European countries, making the seasonality of RES droughts  
 509 critical for the sizing of reserve capacity. Our results show that selecting  
 510 the wrong dataset could severely underestimate RES droughts during winter  
 511 months, thereby affecting the reliability of the energy system during critical  
 512 periods. Additionally, the integration of large shares of solar PV in the system  
 513 leads to a generalised reduction of RES droughts, yet winter months present  
 514 a slight increase. The natural limitations of solar PV lead to inevitably  
 515 higher reserve capacity needs during winter months as reliance on RES in-  
 516 creases. These types of insights are essential to develop targeted strategies  
 517 that enhance grid resilience and ensure a stable energy supply throughout  
 518 the year.

## 519 5. Conclusions

520 This study aimed to answer two key questions: Do generic datasets have  
521 sufficient skill to reliably quantify RES drought events? How does the inte-  
522 gration of solar PV into a predominantly wind-based system alter the char-  
523 acteristics of RES droughts? To address these questions, three datasets were  
524 compared: two derived from the European C3S-Energy dataset, and one de-  
525 veloped by the authors. The datasets derived from C3S-Energy differ in their  
526 assumptions, one assumes a homogeneous distribution of wind and solar PV  
527 capacity across the region, while the other includes the actual locations of  
528 RES farms. The dataset developed by the authors uses a regionally validated  
529 model which accounts for farm locations and uses tailored wind and solar PV  
530 models selected to represent the actual generation.

531 Our results demonstrate that datasets without regional validation mis-  
532 represent the frequency and duration of RES drought events due to their  
533 limited ability to reproduce the observations. The inclusion of wind and so-  
534 lar PV farm locations has limited impact on RES drought analysis compared  
535 to the choice of wind turbine power curves and solar PV models. Whereas  
536 all three datasets capture broad trends in the duration and seasonality of  
537 RES drought events, the actual number of events is consistently underesti-  
538 mated by the non-validated datasets. This effect becomes clearer for extreme  
539 events, as not using regionally validated datasets can yield an overestimation  
540 of the return periods of RES droughts. This can lead to insufficient reserve  
541 capacity planning and potential risks to grid stability and security of supply.

542 The effect of ~~the integration of adding solar PV capacity in a wind-dominated~~  
543 ~~system on RES droughts to a wind dominated power system, as is currently~~  
544 happening in Northwestern Europe, has been explored in the context of RES  
545 droughts. Our analysis has demonstrated that transitioning to a system  
546 with more equal amounts of wind and solar PV capacity reduces the occur-  
547 rence of RES drought events, mitigates extreme RES drought conditions and  
548 enhances overall system resilience. This improvement is attributed to the  
549 complementary nature of wind and solar PV generation, as solar PV gener-  
550 ation typically peaks in summer while wind generation predominates during  
551 winter. However, this integration is unable to counter critical winter RES  
552 droughts, which coincide with the strongest electricity demand in Northern  
553 European countries.

554 The results presented in this study have three main limitations. First,  
555 the definition of RES droughts based on generation does not consider the



important role of demand, which could be of interest to system operators. Second, recent solar PV capacity expansions have changed the generation profile, limiting solar PV data for model training to a single year, although a longer validation period would be preferable. Third, the source for weather data is ERA5 [which](#) has limited spatial resolution, an issue that can be addressed once higher resolution datasets become available.

Future work is planned to extend the current analysis. First, climate projection data will be integrated with different energy scenarios, incorporating the addition of offshore wind, to better understand how climate change and offshore wind may affect RES droughts. Second, expanding the geographic domain of the study to include the rest of Europe, while also including the role of electricity interconnects between countries, would provide a more comprehensive understanding of RES droughts. This would require extensive verification across other European countries, making it a more complex but highly relevant challenge.

## Data Availability

The ERA5 data can be obtained from the Climate Data Store (<https://doi.org/10.24381/cds.adbb2d47>). The C3SE dataset is also available from the Climate Data Store (<https://doi.org/10.24381/cds.4bd77450>). Information on wind and solar PV farms in Ireland can be obtained from the EirGrid website (<https://www.eirgrid.ie/grid/system-and-renewable-data-reports>). The Atlite model used in this study is open-source and can be found on GitHub (<https://github.com/pypsa/atlite>). The data and code required to reproduce the analysis in this article will be made available upon acceptance of the manuscript in a public GitHub repository.

## Acknowledgments

The research conducted in this publication was funded by Science Foundation Ireland and co-funding partners under grant number 21/SPP/3756 through the NexSys Strategic Partnership Programme.

## References

- [1] EuroStat, Renewable Energy Statistics, 2023. URL: [https://ec.europa.eu/eurostat/statistics-explained/index.php?title=Renewable\\_energy\\_statistics](https://ec.europa.eu/eurostat/statistics-explained/index.php?title=Renewable_energy_statistics), Accessed: 2024-11-06.

- 589 [2] I. Staffell, S. Pfenninger, The increasing impact of weather on electricity  
590 supply and demand, *Energy* 145 (2018) 65–78.
- 591 [3] F. Kaspar, M. Borsche, U. Pfeifroth, J. Trentmann, J. Drücke, P. Becker,  
592 A climatological assessment of balancing effects and shortfall risks of  
593 photovoltaics and wind energy in germany and europe, *Advances in*  
594 *Science and Research* 16 (2019) 119–128. doi:10.5194/asr-16-119-2  
595 019.
- 596 [4] F. Mockert, C. M. Grams, T. Brown, F. Neumann, Meteorological  
597 conditions during periods of low wind speed and insolation in Germany:  
598 The role of weather regimes, *Meteorological Applications* 30 (2023)  
599 e2141. doi:10.1002/met.2141.
- 600 [5] M. Ohba, Y. Kanno, D. Nohara, Climatology of dark doldrums in japan,  
601 *Renewable and Sustainable Energy Reviews* 155 (2022) 111927. doi:10  
602 .1016/j.rser.2021.111927.
- 603 [6] M. J. Mayer, B. Biró, B. Szücs, A. Aszódi, Probabilistic modeling of  
604 future electricity systems with high renewable energy penetration using  
605 machine learning, *Applied Energy* 336 (2023) 120801. doi:10.1016/j.  
606 apenergy.2023.120801.
- 607 [7] D. Raynaud, B. Hingray, B. François, J. Creutin, Energy droughts from  
608 variable renewable energy sources in European climates, *Renewable*  
609 *Energy* 125 (2018) 578–589. doi:https://doi.org/10.1016/j.renene  
610 .2018.02.130.
- 611 [8] A. Gangopadhyay, A. K. Seshadri, N. J. Sparks, R. Toumi, The role  
612 of wind-solar hybrid plants in mitigating renewable energy-droughts,  
613 *Renewable Energy* 194 (2022) 926–937. doi:10.1016/j.renene.2022.  
614 05.122.
- 615 [9] J. Kapica, J. Jurasz, F. A. Canales, H. Bloomfield, M. Guezgouz,  
616 M. De Felice, Z. Kobus, The potential impact of climate change on  
617 european renewable energy droughts, *Renewable and Sustainable En-*  
618 *ergy Reviews* 189 (2024) 114011. doi:10.1016/j.rser.2023.114011.
- 619 [10] K. Z. Rinaldi, J. A. Dowling, T. H. Ruggles, K. Caldeira, N. S. Lewis,  
620 Wind and Solar Resource Droughts in California Highlight the Benefits

- of Long-Term Storage and Integration with the Western Interconnect,  
Environmental Science and Technology 55 (2021) 6214–6226. doi:10.1021/acs.est.0c07848.
- [11] P. T. Brown, D. J. Farnham, K. Caldeira, Meteorology and climatology of historical weekly wind and solar power resource droughts over western North America in ERA5, SN Applied Sciences 3 (2021) 814. doi:10.1007/s42452-021-04794-z.
- [12] S. Allen, N. Otero, Standardised indices to monitor energy droughts, Renewable Energy 217 (2023) 119206. doi:10.1016/j.renene.2023.119206.
- [13] C. Bracken, N. Voisin, C. D. Burleyson, A. M. Campbell, Z. J. Hou, D. Broman, Standardized benchmark of historical compound wind and solar energy droughts across the Continental United States, Renewable Energy 220 (2024) 119550. doi:https://doi.org/10.1016/j.renene.2023.119550.
- [14] H. Lei, P. Liu, Q. Cheng, H. Xu, W. Liu, Y. Zheng, X. Chen, Y. Zhou, Frequency, duration, severity of energy drought and its propagation in hydro-wind-photovoltaic complementary systems, Renewable Energy (2024) 120845. doi:10.1016/j.renene.2024.120845, 2.
- [15] H. Hersbach, B. Bell, P. Berrisford, S. Hirahara, A. Horányi, J. Muñoz-Sabater, J. Nicolas, C. Peubey, R. Radu, D. Schepers, et al., The ERA5 global reanalysis, Quarterly Journal of the Royal Meteorological Society 146 (2020) 1999–2049. doi:10.1002/qj.3803.
- [16] L. Dubus, Y. Saint-Drenan, A. Troccoli, M. De Felice, Y. Moreau, L. Ho-Tran, C. Goodess, R. Amaro E Silva, L. Sanger, C3S Energy: A climate service for the provision of power supply and demand indicators for Europe based on the ERA5 reanalysis and ENTSO-E data, Meteorological Applications 30 (2023) e2145. doi:10.1002/met.2145.
- [17] F. Hofmann, J. Hampp, F. Neumann, T. Brown, J. Hörsch, Atlite: a lightweight Python package for calculating renewable power potentials and time series, Journal of Open Source Software 6 (2021) 3294. doi:10.21105/joss.03294.

- 653 [18] A. Kies, B. U. Schyska, M. Bilousova, O. El Sayed, J. Jurasz,  
654 H. Stoecker, Critical review of renewable generation datasets and their  
655 implications for european power system models, *Renewable and Sus-*  
656 *tainable Energy Reviews* 152 (2021) 111614. doi:10.1016/j.rser.202  
657 1.111614.
- 658 [19] EirGrid & SONI, System and Renewable Data Reports, 2023. URL:  
659 [https://www.eirgrid.ie/grid/system-and-renewable-data-rep](https://www.eirgrid.ie/grid/system-and-renewable-data-reports)  
660 [orts](https://www.eirgrid.ie/grid/system-and-renewable-data-reports), Accessed: 2024-11-06.
- 661 [20] Y.-M. Saint-Drenan, L. Wald, T. Ranchin, L. Dubus, A. Troccoli, An  
662 approach for the estimation of the aggregated photovoltaic power gener-  
663 ated in several European countries from meteorological data, *Advances*  
664 *in Science and Research* 15 (2018) 51–62. doi:10.5194/asr-15-51-201  
665 8.
- 666 [21] I. Staffell, S. Pfenninger, Using bias-corrected reanalysis to simulate  
667 current and future wind power output, *Energy* 114 (2016) 1224–1239.  
668 doi:10.1016/j.energy.2016.08.068.
- 669 [22] Government of Ireland, Climate Action Plan 2024, Technical Report 3,  
670 Department of the Environment, Climate and Communications, 2023.  
671 URL: [https://www.gov.ie/pdf/?file=https://assets.gov.ie/](https://www.gov.ie/pdf/?file=https://assets.gov.ie/284675/70922dc5-1480-4c2e-830e-295afd0b5356.pdf)  
672 [284675/70922dc5-1480-4c2e-830e-295afd0b5356.pdf](https://www.gov.ie/pdf/?file=https://assets.gov.ie/284675/70922dc5-1480-4c2e-830e-295afd0b5356.pdf), Accessed:  
673 2024-11-06.
- 674 [23] Sustainable Energy Authority Ireland, National Energy Projections  
675 2024, Technical Report, Sustainability Energy Authority of Ireland,  
676 2024. URL: [https://www.seai.ie/news-and-events/news/energ](https://www.seai.ie/news-and-events/news/energy-projections-report)  
677 [y-projections-report](https://www.seai.ie/news-and-events/news/energy-projections-report), Accessed: 2024-11-06.
- 678 [24] EirGrid & SONI, Tomorrow’s Energy Scenarios 2023, Technical Report,  
679 EirGrid & SONI, 2023. URL: [https://cms.eirgrid.ie/sites/def](https://cms.eirgrid.ie/sites/default/files/publications/TES-2023-Final-Full-Report.pdf)  
680 [ault/files/publications/TES-2023-Final-Full-Report.pdf](https://cms.eirgrid.ie/sites/default/files/publications/TES-2023-Final-Full-Report.pdf),  
681 Accessed: 2024-11-06.
- 682 [25] H. G. Beyer, G. Heilscher, S. Bofinger, A robust model for the mpp  
683 performance of different types of pv-modules applied for the performance  
684 check of grid connected systems, *Eurosun* (2004) 8.